Applied Physics Letters ARTICLE scitation.org/journal/apl

# Electrical characterization of GaN Schottky barrier diode at cryogenic temperatures

Cite as: Appl. Phys. Lett. **116**, 062102 (2020); doi: 10.1063/1.5131337
Submitted: 12 October 2019 · Accepted: 24 January 2020 ·
Published Online: 10 February 2020



Jiaxiang Chen,[1,2,3] Min Zhu,[1,2,3] Xing Lu,[4,a)] and Xinbo Zou[1,b)]

## AFFILIATIONS

[1]School of Information Science and Technology, ShanghaiTech University, 201210 Shanghai, China
[2]University of Chinese Academy of Sciences, 100049 Beijing, China
[3]Shanghai Institute of Microsystem and Information Technology, Chinese Academy of Sciences, 200050 Shanghai, China
[4]School of Electronics and Information Technology, Sun Yat-sen University, 510006 Guangzhou, China

[a)]Electronic mail: eexlu@connect.ust.hk
[b)]Author to whom correspondence should be addressed: zouxb@shanghaitech.edu.cn

## ABSTRACT

In this report, electrical characteristics of the Ni/GaN Schottky barrier diode grown on sapphire have been investigated in the range of 20 K–300 K, using current–voltage, capacitance–voltage, and deep level transient spectroscopy (DLTS). A unified forward current model, namely a modified thermionic emission diffusion model, has been developed to explain the forward characteristics, especially in the regime with a large ideality factor. Three leakage current mechanisms and their applicability boundaries have been identified for various bias conditions and temperature ranges: Frenkel–Poole emission for temperatures above 110 K; variable range hopping (VRH) for 20 K–110 K, but with a reverse bias less than 20 V; high-field VRH, in a similar form of Fowler–Nordheim tunneling, for cryogenic temperatures below 110 K, and relatively large bias (>25 V). Four trap levels with their energy separations from the conduction band edge of $0.100 \pm 0.030$ eV, 0.300 eV, 0.311 eV, and 0.362 eV have been tagged together with their capture cross sections and trap concentrations. The significantly reduced DLTS signal at 100 K suggested that traps practically became inactive at cryogenic temperatures, thus greatly suppressing the trap-assisted carrier hopping effects.



Investigations of solid-state device performance at extremely low temperatures[1,2] are of great interest in on-board electronics used in satellites and space missions to outer planets. At low temperatures, solid-state devices are expected to have higher carrier mobility and lower leakage current to enhance device performance, which would favor the adoption of cryogenic electronics for superconducting electronics, cryo-imaging, and future data centers.[3] Gallium nitride (GaN) devices can be used in harsh environments owing to the high chemical and mechanical stability, wide energy bandgap, high electron mobility, and large critical electrical field of GaN. As building blocks of III-N electronics, GaN-based Schottky barrier diodes (SBDs) have attracted considerable interest due to their low turn-on voltage, low on-resistance, and outstanding rectifying performance.[4–8]

Temperature dependent current–voltage measurements of GaN SBDs were extensively performed for a wide temperature range starting from 40 K.[7] Device parameters, including the ideality factor and Schottky barrier height (SBH, $\phi_B$), were extracted and studied using the thermionic emission (TE) model or thermionic field emission (TFE) mode.[5,8,9] It was found that the ideality factor was increased to nearly five as the temperature was decreased to 40 K.[7] There is still considerable ambiguity with regard to the $\phi_B$-temperature relationship discrepancy extracted by capacitance–voltage ($C$–$V$) and $I$–$V$ methods.[6,10] The barrier height $\phi_B$ extracted from the $I$–$V$ characteristics was decreased as the decreased temperature, which, however, contradicted the $\phi_B$-temperature relationship extracted from the $C$–$V$ measurement results.[11] Recently, Maeda *et al.* measured the vertical SBD on free standing GaN substrates from 223 K up to 573 K and used the thermionic emission diffusion (TED) model to correlate the SBH extracted from $I$–$V$ to that from $C$–$V$ methods.[11] However, the applicability of the TED model at cryogenic temperatures and non-ideal $I$–$V$ regimes is still unclear.

There have been reports studying leakage current mechanisms of Schottky contact[12–14] to AlGaN/GaN and GaN grown by molecular-beam epitaxy (MBE). Frenkel–Poole emission (FPE) could well explain the leakage current at relatively high temperatures (e.g., $T > 150$ K), while it was believed that tunneling was the dominant mechanism at low temperatures. One main limitation of the above measurements was that they were carried out at a reverse bias no larger than 10 V, preventing revealing the leakage current mechanism in a relatively high bias range, which is important for wide energy bandgap semiconductors.[15,16]

Despite the steady advance in the understanding and operation of GaN SBDs for low-temperature applications, there are still several relevant issues to be addressed: (1) at cryogenic temperatures, the $I$–$V$ characteristics became nonideal as indicated by a sharp increase in ideality factors. A single model that can well describe the $I$–$V$ characteristics especially at cryogenic temperatures is needed, without using an arguably discrepant barrier height; (2) for reverse leakage current analysis, it was conventional to study the effects of temperature and limit the bias to no large than 10 V. However, the leakage mechanisms under high reverse bias, which is commonly used for GaN devices,[16,17] was not fully understood especially at cryogenic temperatures; (3) the performance of GaN SBD at a temperature of 40 K or even lower has not been reported and evaluated yet.

In this work, forward characteristics of the Ni/GaN SBD were measured from 20 K to 300 K, proving its capability of working at extremely low temperatures. A single unified model that took barrier height inhomogeneity into account was developed, and the level of inhomogeneity was correlated with the value of the ideality factor. In this model, the forward current in the range 20 K–300 K could be well described, and the temperature-dependent carrier mobility can be extracted. The leakage current was measured from 20 K to 300 K as well with reverse biases up to 30 V. It was found that the reverse conduction was bias dependent for temperatures below 110 K. Capacitance based deep level transient spectroscopy (DLTS) was also utilized to partially correlate the trap properties with the leakage current mechanisms at cryogenic temperatures (Figs. 1 and 2).

As shown as in Fig. 1, the SBD mesa with a diameter of 500 $\mu$m was formed by inductively coupled plasma (ICP) etching, and the diode was fabricated using Ni/Au for Schottky contact and Ti/Al/Ni/Au for Ohmic contact. For low-temperature and temperature-dependent measurements, the sample was put inside a cryostat cooled by liquid helium.

As shown in Fig. 2, the temperature-dependent $C$–$V$ measurements were performed at 1 MHz, sufficiently high to exclude the contribution of the interface state charges, especially those holding long time constants. The $C$–$V$ characteristics were used to extract the built-in potential $V_{bi}$ using the depletion capacitance approximation and corresponding $\phi_{B-CV}$ by the following equations:

$$\frac{1}{C^2} = \frac{2}{\varepsilon q F^2 N_s}\left(V + V_{bi} - \frac{kT}{q}\right), \tag{1}$$

$$q\phi_{B-CV} = qV_{bi} + (E_C - E_F) + kT, \tag{2}$$

where $N_s$ is the net donor concentration, $F$ is the area of Schottky contact, $\varepsilon$ is the dielectric constant of GaN (10.4 $\varepsilon_0$), $q$ is the elementary charge, $k$ is the Boltzmann constant, $T$ is the Kelvin temperature, $E_C$ is the conduction band minimum of GaN, and $E_F$ is the Fermi level. As

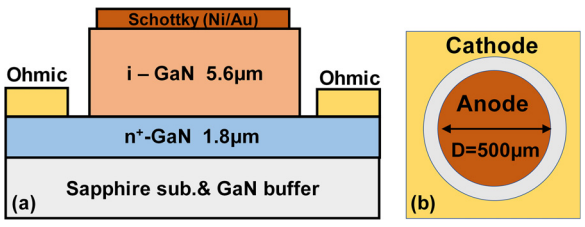


**FIG. 1.** Schematic illustrations of the GaN quasi-vertical Schottky barrier diode: (a) cross-sectional view and (b) top view.

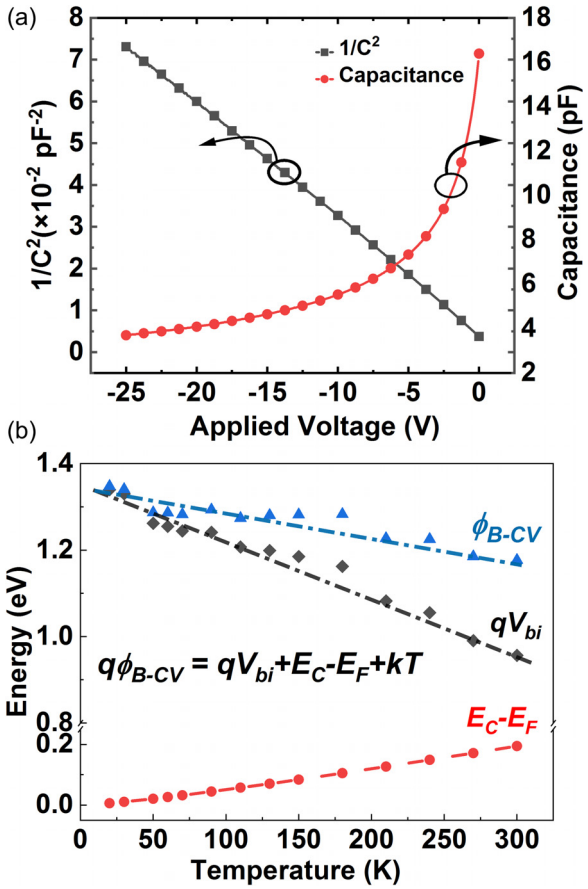


**FIG. 2.** (a) Voltage-dependent capacitance and $1/C^2$-$V$ plot of the GaN Schottky barrier diode at 20 K. (b) Temperature-dependent built-in potential ($V_{bi}$) determined by the linear extrapolation of the $C$–$V$ measurement results and the corresponding Schottky barrier height $\phi_{B-CV}$ in the range of 20 K–300 K.

the temperature was decreased from 300 K to 20 K, $\phi_{B-CV}$ was increased slightly from 1.17 eV to 1.36 eV, which matched with the increased threshold voltage of SBD at lowered temperatures.

Figures 3(a) and 3(b) show the forward $J$–$V$ characteristics of the GaN SBD from 20 K to 300 K. The diode could be turned on even at 20 K. The threshold voltage was increased from 0.67 V to 1.03 V, given 1 A/cm$^2$ as the threshold current density as the temperature decreased from 300 K to 20 K. The ideality factor, $n$, which is defined as $n = q(dV/dlnJ)/kT$, was gradually increased from 1.05 at 300 K to 2.24 at 90 K, but increased sharply to 12.6 at 20 K. Despite the increased ideality factor, the differential $R_{on}$ at 20 mA was steadily decreased from 22.2 m$\Omega$ cm$^2$ at 300 K to 16.6 m$\Omega$ cm$^2$ at 20 K, due to the enhanced carrier mobility.

Previous reports on the operations of SBD at low temperatures typically used the TE or the TFE model[8,18,19] to describe the temperature-dependent $I$–$V$ behaviors. It is quite often concluded that the barrier height has a positive temperature coefficient, which is of the opposite sign of that extracted from $C$–$V$ measurements, expressed as $\phi_{B-CV}$.

$\phi_{B-CV}$ is insensitive to potential fluctuations on a length scale of less than the space charge region as the $C$–$V$ method averages over the

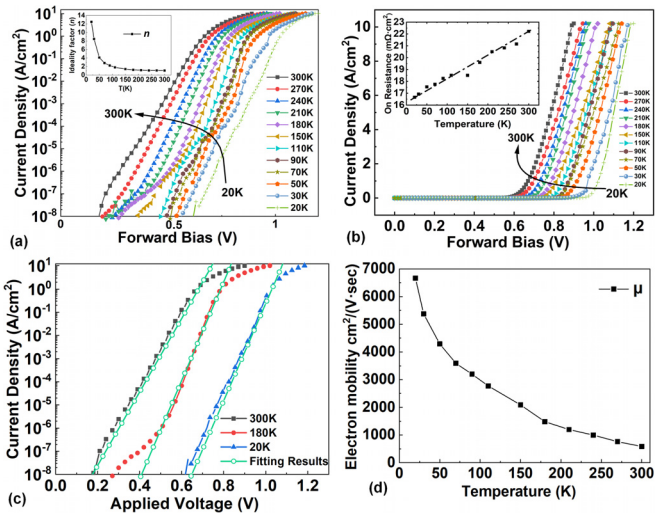


**FIG. 3.** Forward *J–V–T* characteristics on a semi-log scale (a) and a linear scale (b) in the range of 20 K–300 K. Insets: (a) temperature dependent ideality factor, (b) differential on-resistance ($R_{on}$) at an injection current of 20 mA, (c) fitting of forward current at three typical temperature steps using the modified TED model, and (d) temperature-dependent carrier mobility extracted from the modified TED model.

whole Schottky area.[20] $\phi_{B-CV}$ is not applicable to study the carrier transport and *I–V* characteristics, as the carriers tend to move by going over the lowest barrier height $\phi_{B-low}$. The Schottky barrier inhomogeneity has been regarded being originated from interface state density $N_{SS}$, which is also related to the ideality factor using $n = 1 + \frac{d}{\varepsilon_i}\left[\frac{\varepsilon_s}{w} + qN_{SS}\right]$, where $d$ is the thickness of the interfacial layer, $\varepsilon_s$ and $\varepsilon_i$ are the permittivity of the semiconductor and the permittivity of the interfacial layer, $N_{SS}$ denotes the density of interface states, while other constants have their own common meanings.[10,21,22]

Thus, we proposed to use ideality factor $n$ as the numerical indicator of Schottky barrier inhomogeneity, and the effective $\phi_{B-low}$ could be expressed as $\frac{\phi_{B-CV}}{n}$, which is the height that electrons have to go over for transport.

Considering the dual interpretation of the ideality factor, the level of deviation from the ideal *J–V* curve, and the numerical indicator of Schottky barrier inhomogeneity, the ideality factor has been included for both exponential terms in Eq. (3), rather than ideality factor inclusion in the exponential term associated with the applied voltage *V* only[4]

$$J_{TED} = \frac{A^* T^2}{1 + \nu_R/\nu_D} \exp\left(-\frac{q\phi_{B-CV}}{nkT}\right)\left[\exp\left(\frac{qV}{nkT}\right) - 1\right], \quad (3)$$

where $\nu_R$ is the thermal velocity $\nu_R = \frac{A^* T^2}{qN_C}$, $\nu_D$ denotes the diffusion velocity, approximated by $\nu_D = \mu E_m$, $A^*$ is the Richardson constant (26.5 A cm$^{-2}$ K$^{-2}$ for GaN[9]), and $n$ is the ideality factor calculated from the slope of *J–V–T* characteristics.

Figure 3(c) shows the measured *J–V* characteristics and fitted curves using Eq. (3), at three temperature steps, namely, 20 K, 180 K, and 300 K. The modified TED model could well fit the current density increase in a wide temperature range by introducing ideality factors for the two exponential terms associated with SBH and applied voltage *V*. This method may also be used to model the dataset in some other literature studies, particularly at low temperatures and in high ideality factor regimes.[10] By using the SBH extracted from *C–V* measurements and through fitting, the low-field carrier mobility could be extracted, as shown in Fig. 3(d). At 300 K, the mobility extracted was 585 cm$^2$/v s[4] and increased to 6800 cm$^2$/v s as it decreased to 20 K. The electron mobility is as follows: $\mu = \mu_{300}\left(\frac{T}{300}\right)^{\gamma}$, where $\gamma$ is the temperature dependence parameter to describe the decay in mobility. $\gamma$ was determined to be −0.92, comparable to −1.5 reported elsewhere.[23] A further examination of the modified TED model indicated that by including ideality factors for both exponential terms, the TED model would behave similar to a modified TE model at cryogenic temperatures down to 20 K, as $1 + \nu_R/\nu_D$ was approximately equal to unity. At relatively higher temperatures, one had to take $1 + \nu_R/\nu_D$ into account as the sum was not close to unity any more.

Figure 4(a) shows the leakage current density for reverse biases up to 30 V in the range of 20 K–300 K. At 300 K, $I_{leak}$ was only 140 nA at −30 V, whose corresponding leakage current density was $7.6 \times 10^{-5}$ A/cm$^2$. At 20 K, $I_{leak}$ was suppressed by more than one order at −30 V. In order to investigate the mechanisms, the reverse current density was re-plotted as a function of the reciprocal temperature, as shown in Fig. 5(a). Figure 5(a) shows the evolution of the reverse current density with the reciprocal temperature, and two regions have been identified: relatively high temperature region (T > 110 K, shaded region) and relatively low temperature region (T < 110 K, unshaded region). In the shaded region, $J_{leak}$ was decreased rapidly with decreasing temperature from 300 K to 110 K. Furthermore, the data collected above 110 K (shaded region) are re-plotted in Fig. 5(b), in which the plot of *J*/*E* as a function of $E^{1/2}$ on a semi-log scale shows a linear relationship for the complete negative bias range up to −30 V, confirming that Frenkel–Poole emission (FPE) was the main mechanism of the leakage current above 110 K, according to the FPE model as follows:[4]

$$Ln\left(\frac{J}{E}\right) = \frac{q}{KT}\sqrt{\frac{qE}{\pi\varepsilon_0\varepsilon_s}} - \frac{q\phi_B}{kT} + LnC. \quad (4)$$

For the temperature below 110 K [unshaded region in Fig. 5(a)], the leakage current–temperature dependence could be further divided into two parts, low bias part and high bias part. At −5 V and −10 V, the leakage current was gradually decreased from 110 K to 20 K. The conduction could be well fitted by the variable range hopping (VRH) model proposed by Hill[24] and Mott[25]

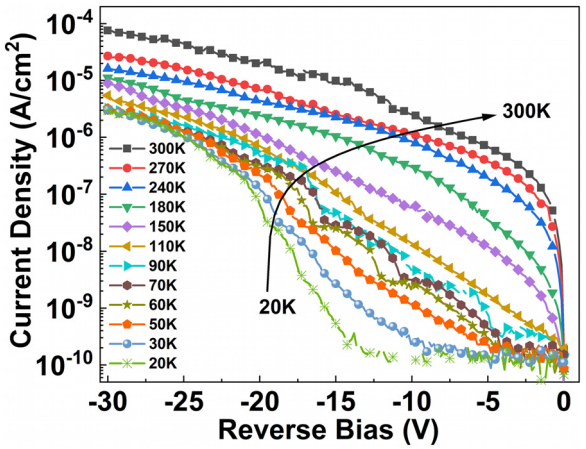


**FIG. 4.** Temperature-dependent *J–V* characteristics up to a reverse bias of 30 V.

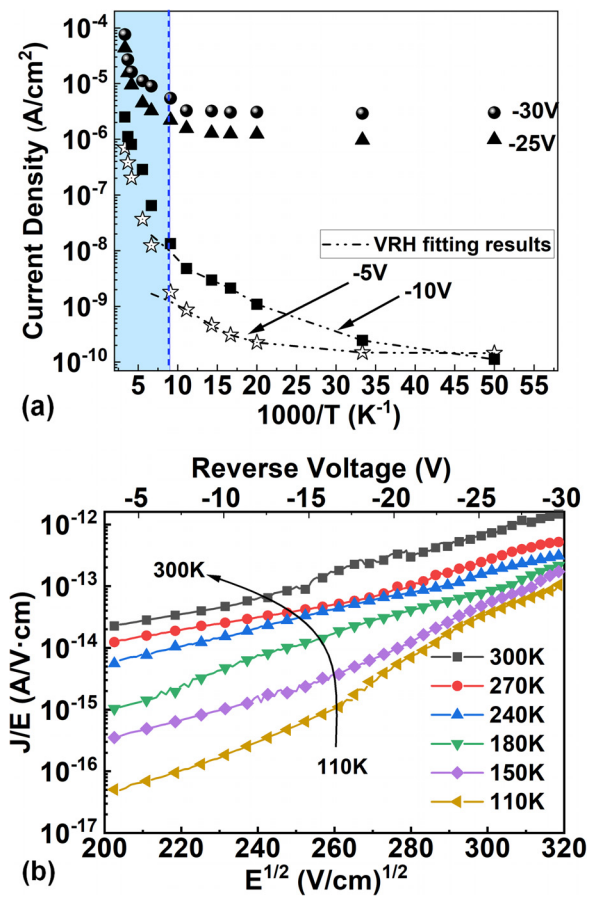


FIG. 5. (a) The leakage current as a function of reciprocal temperatures for various bias levels from −5 V to −30 V. The dashed-dotted lines denote VRH fitting results. (b) Re-plotting of data points in the shaded region of (a).

$$J \propto \exp\left[-C\left(\frac{T_{VRH}}{T}\right)^{\frac{1}{4}}\left\{1 - C'E^2/T^{\frac{1}{2}}\right\}\right], \quad (5)$$

where C and C′ are constants and $T_{VRH}$ is the characteristic temperature, which determines the slope of the curve, as shown by the fitting curves in Fig. 5(a).

A further examination of the leakage current, as shown in Fig. 6(a), for each measurement temperature at 110 K, shows that the current density $J$ was found to be linearly proportional to $E^2$ on a semi-log scale, confirming that the VRH mechanism was the governing mechanism of the leakage current. As the bias was enhanced, high field VRH started to dominate the reverse current. Thus, one may find reverse current independent of the temperatures for bias from −25 V to −30 V, as shown in Figs. 5(a) and 6(b). In Fig. 6(b), $J/E^2$ as a function of the reciprocal electrical field is plotted, indicating that high field VRH, which has a similar form of Fowler–Nordheim (FN) tunneling, was the main reason for reverse conduction[12,24]

$$\mathrm{J} = AE^2\exp\left(-\frac{B}{E}\right), \quad (6)$$

where both $A$ and $B$ are constants, barely dependent on temperatures.

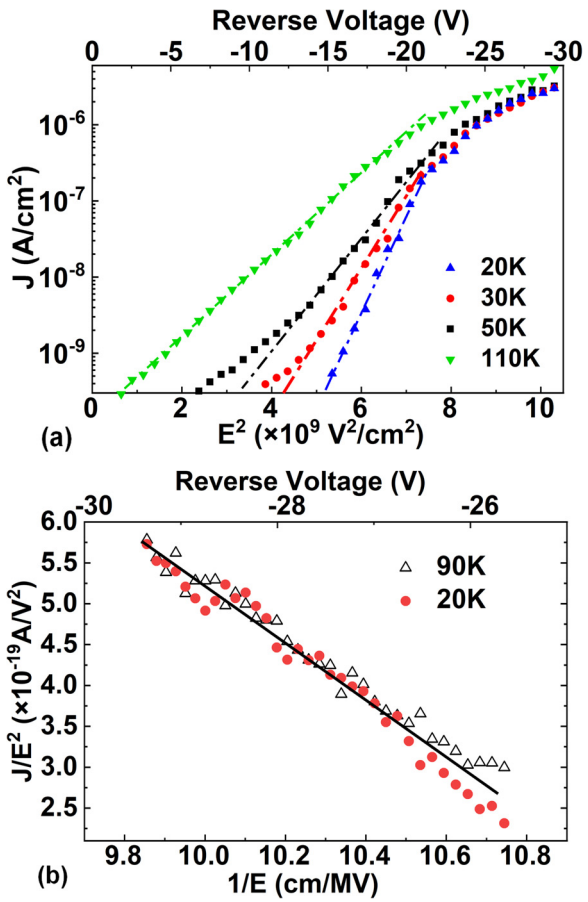


FIG. 6. (a) Leakage current density as a function of $E^2$ for temperatures below 110 K. (b) $J/E^2$ vs $1/E$ in the voltage range from −25 V to −30 V at 90 K and 20 K.

It is commonly believed that traps in the GaN SBD are the main sources of leakage current, such as via electrons hopping from one trap to another. The DLTS signal spectra were obtained in the temperature range of 50 K–300 K with 5 K per step. Four electron traps labeled as E1, E2, E3, and E4 are extracted by DLTS, as shown in Fig. 7(b) and Table I. E2 and E3 shared similar activation energy due to the overlapping of DLTS peaks. The energy level of E2 and E3 is commonly observed for GaN grown on sapphire.[26,27] E2 and E3 held

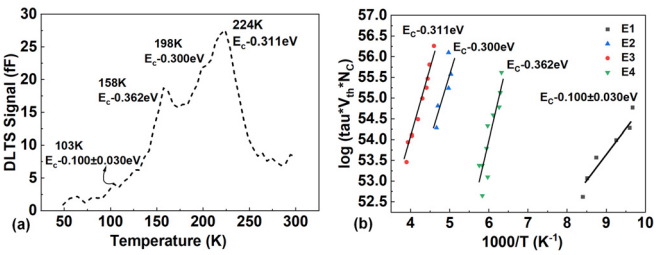


FIG. 7. (a) DLTS spectra of GaN SBD on sapphire from 50 K to 300 K. (b) Arrhenius plot of four electron traps labeled as E1, E2, E3, and E4.

**TABLE I.** Properties of four trap levels extracted from DLTS.

| Trap No. | $E_C - E_T$ (eV) | $\sigma \times 10^{-19}$ (cm$^2$) | $N_T \times 10^{13}$ (/cm$^3$) |
|---|---|---|---|
| E1 | $0.100 \pm 0.030$ | 0.6–6.4 | 1.28–1.41 |
| E2 | 0.300 | 237.0 | 7.25 |
| E3 | 0.311 | 66.9 | 9.47 |
| E4 | 0.362 | $3.1 \times 10^6$ | 5.57 |

the two largest trap concentrations among the four observed, indicating their dominance for trap-assisted leakage, especially $T > 200$ K.

The trap E1 has been often observed and reported for Si-doped and undoped GaN samples,[28] with a similar trap concentration. It is believed that both point defects, namely, nitrogen vacancy ($V_N$) induced during growth[28] and fabrication,[29] could be the origin of such a relatively shallow trap. The trap E4 was found to have an activation energy of 0.362 eV, close to a similar level, which has been connected to etching-induced damages in the literature.[30] As shown in Fig. 7(a), the significantly reduced DLTS signal indicated that traps practically became inactive at cryogenic temperatures below 100 K, and thus, the trap-assisted hopping effect, as well as leakage current associated with it, was suppressed.

In summary, electrical characteristics of Ni/GaN SBD have been investigated from 20 K to 300 K. A unified model, namely, a modified TED model, has been developed to explain the forward characteristics, especially in the regime with large ideality factors. In this modified model, the ideality factor was included for the exponential terms associated with SBH and applied voltage as the ideality factor has been proposed as a numerical indicator of Schottky barrier inhomogeneity, in addition to the conventional level of deviation from ideal $I$–$V$ characteristics. The analysis of leakage current mechanisms took the bias level into account in addition to the impact of temperatures. For $T > 110$ K, FPE effects were determined as the main reason for reverse conduction. However, for $T < 110$ K, the leakage could be explained by VRH from 0 to 20 V, and the leakage current was governed by the high-field VRH model, which has a similar form of FN tunneling, for bias from $-25$ V to $-30$ V. Four trap levels have been tagged using capacitance-based DLTS, with activation energy, capture cross sections, and trap densities being revealed. The significantly reduced DLTS signal at 100 K suggested that traps practically became inactive at cryogenic temperatures, and thus, the trap-assisted hopping effect and the resulting leakage current were suppressed.

See the supplementary material for the detailed temperature-dependent capacitance–voltage ($C$–$V$) measurement data that illustrate the process of deriving $V_{bi}$, which was used to link the corresponding Schottky barrier height $\phi_{B-CV}$, as shown in Fig. 2.

This work was supported by ShanghaiTech University Startup Fund and sponsored by Shanghai Pujiang Program No. 18PJ1408200, the Shanghai Eastern Scholar (Youth) Program, and the CAS Strategic Science and Technology Program under Grant No. XDA18000000.

## REFERENCES

[1]M. D. Henry, S. W. Smith, R. M. Lewis, and J. F. Ihlefeld, Appl. Phys. Lett. **114**(9), 092903 (2019).
[2]P. Gehring, M. van der Star, C. Evangeli, J. J. Le Roy, L. Bogani, O. V. Kolosov, and H. S. J. van der Zant, Appl. Phys. Lett. **115**(7), 073103 (2019).
[3]E. Dogmus, R. Kabouche, S. Lepilliet, A. Linge, M. Zegaoui, H. Ben-Ammar, M.-P. Chauvat, P. Ruterana, P. Gamarra, C. Lacam, M. Tordjman, and F. Medjdoub, Electronics **5**(4), 31 (2016).
[4]K. R. Peta, B.-G. Park, S.-T. Lee, M.-D. Kim, J.-E. Oh, T.-G. Kim, and V. R. Reddy, Thin Solid Films **534**, 603 (2013).
[5]N. Yıldırım, K. Ejderha, and A. Turut, J. Appl. Phys. **108**(11), 114506 (2010).
[6]V. S. Nirwal and K. R. Peta, Mater. Res. Express **3**(12), 125901 (2016).
[7]S. Doğan, S. Duman, B. Gürbulak, S. Tüzemen, and H. Morkoç, Physica E **41**(4), 646 (2009).
[8]İ. Dökme, Microelectron. Reliab. **51**(2), 360 (2011).
[9]E. Arslan, S. Bütün, Y. Şafak, H. Çakmak, H. Yu, and E. Özbay, Microelectron. Reliab. **51**(3), 576 (2011).
[10]V. Rajagopal Reddy and N. Nanda Kumar Reddy, Superlattices Microstruct. **52**(3), 484 (2012).
[11]T. Maeda, M. Okada, M. Ueno, Y. Yamamoto, T. Kimoto, M. Horita, and J. Suda, Appl. Phys. Express **10**(5), 051002 (2017).
[12]H. Zhang, E. J. Miller, and E. T. Yu, J. Appl. Phys. **99**(2), 023703 (2006).
[13]P. K. Rao, B. Park, S.-T. Lee, Y.-K. Noh, M.-D. Kim, and J.-E. Oh, J. Appl. Phys. **110**(1), 013716 (2011).
[14]W. Jin Ha, S. Chhajed, S. Jae Oh, S. Hwang, J. Kyu Kim, J.-H. Lee, and K.-S. Kim, Appl. Phys. Lett. **100**(13), 132104 (2012).
[15]Y. Cao, R. Chu, R. Li, M. Chen, R. Chang, and B. Hughes, Appl. Phys. Lett. **108**(6), 062103 (2016).
[16]S. Usami, A. Tanaka, H. Fukushima, Y. Ando, M. Deki, S. Nitta, Y. Honda, and H. Amano, Jpn. J. Appl. Phys., Part 1 **58**(SC), SCCB24 (2019).
[17]Y. Zhou, D. Wang, C. Ahyi, C.-C. Tin, J. Williams, M. Park, N. M. Williams, A. Hanser, and E. A. Preble, J. Appl. Phys. **101**(2), 024506 (2007).
[18]W. Mtangi, P. J. Janse van Rensburg, M. Diale, F. D. Auret, C. Nyamhere, J. M. Nel, and A. Chawanda, Mater. Sci. Eng.: B **171**(1-3), 1 (2010).
[19]S. K. Cheung and N. W. Cheung, Appl. Phys. Lett. **49**(2), 85 (1986).
[20]J. H. Werner and H. H. Güttler, J. Appl. Phys. **69**(3), 1522 (1991).
[21]H. C. Card and E. H. Rhoderick, J. Phys. D **4**(10), 1589 (1971).
[22]E. H. Rhoderick and R. H. Williams, *Metal-Semiconductor Contacts* (Clarendon Press, Oxford, 1988).
[23]H. Tang, W. Kim, A. Botchkarev, G. Popovici, F. Hamdani, and H. Morkoç, Solid-State Electron. **42**(5), 839 (1998).
[24]R. M. Hill, Philos. Mag. **24**(192), 1307 (1971).
[25]N. F. Mott, Philos. Mag. **19**(160), 835 (1969).
[26]Y. Tokuda, in CS MANTECH Conference, Denver, Colorado, USA, 19–22 May 2014.
[27]Y. Tokuda, Y. Matsuoka, H. Ueda, O. Ishiguro, N. Soejima, and T. Kachi, Superlattices Microstruct. **40**(4), 268 (2006).
[28]C. B. Soh, S. J. Chua, H. F. Lim, D. Z. Chi, S. Tripathy, and W. Liu, J. Appl. Phys. **96**(3), 1341 (2004).
[29]Z. Q. Fang, D. C. Look, X. L. Wang, J. Han, F. A. Khan, and I. Adesida, Appl. Phys. Lett. **82**(10), 1562 (2003).
[30]Z. Q. Fang, D. C. Look, P. Visconti, D. F. Wang, C. Z. Lu, F. Yun, H. Morkoç, S. S. Park, and K. Y. Lee, Appl. Phys. Lett. **78**(15), 2178 (2001).